Journal of Applied Fluid Mechanics, Vol. 17, No. 2, pp. 310-321, 2024.
Available online at www.jafmonline.net, ISSN 1735-3572, EISSN 1735-3645.
https://doi.org/10.47176/jafm.17.02.2141

Experimental Study on the Dynamics of a Moving Droplet Impacting a Sessile Droplet

D. Chen, L. Ming, T. Wang, M. Qiu and Z. Lin†

Key Laboratory of Fluid Transmission Technology of Zhejiang Province Zhejiang Sci-Tech University, Hangzhou, 310018, China

† *Corresponding Author Email: linzhe0122@zstu.edu.cn*

ABSTRACT

The phenomenon of droplets impacting droplets is common in many fields including the chemical, nuclear, and aerospace industries. In this paper, high-speed photography technology is used to obtain the variation law and evolution properties exhibited by droplets colliding with sessile droplets of varying sizes. We further explored how the Weber number (*We*) and volume ratio (V_p/V_i) influence the behavior of droplets colliding with sessile droplets. The phenomenon of droplets impacting sessile droplets of different volumes is different from that of droplets impacting liquid films. In terms of droplet spreading, compression and the non-splashing liquid crown, the phenomena and laws reported in the present study are applicable for $1 \leq We \leq 165$ and droplet volume ratios of $1 \leq V_p/V_i \leq 6$. With a low Weber number, the droplet compresses and deforms downward without coalescence at the initial stage of collision. A high Weber number results in a no-splashing liquid crown. These findings provide important insights into the dynamics of droplet-droplet interactions.

Article History

Received July 8, 2023
Revised August 28, 2023
Accepted October 5, 2023
Available online December 4, 2023

Keywords:

Droplet impact
Sessile droplet
Volume ratio
No-splashing liquid crown
Droplet compress

1. INTRODUCTION

Droplet collisions widely exist in many fields including chemical and energy production and the aerospace industry. For example, during plasma spraying, droplets are atomized by a high-speed plasma flow into very fine droplets where the composition of the structure is uniform. Within a kind of internal combustion engine, liquid fuel droplets impact the surface of the piston and the cylinder. In the context of inkjet printing, achieving uniform deposition of ink droplets on the paper is essential. (Bai & Gosman 1995; Lim et al., 2009; Dalili et al., 2014; Zhong et al., 2020).

In numerous instances within these applications, the droplets encounter either a solid substrate or with stationary droplets previously placed on the substrate. (Stone et al., 2004). The dynamic characteristics and morphological features of droplet collision are predominantly shaped by the properties of both the droplet itself and the surface it comes into contact with. (Moghtadernejad et al., 2020). Numerous investigations have centered on the collision of a single droplet on a wall and the controllable variables. With respect to the droplet, the controllable variables include diameter, viscosity, and collision speed as studied by (Deka et al., 2019; Emdadi & Pournaderi, 2019; Qin et al., 2019). Controllable variables for the wall include roughness, wettability, surface type, and microscopic shape as studied by (Liang et al., 2014; Feng, 2017; Li et al., 2019; Bernard et al., 2020; Karn et al., 2020; Luo et al., 2021; Wang et al., 2021). Nevertheless, the interaction between droplets is not considered, so the knowledge gained from the single droplet experiment cannot be directly applied to a real jet collision field (Fujimoto et al., 2008). Thus, several researchers, including (Fujimoto et al., 2008; Farokhirad et al., 2015; Raman et al., 2016; Wakefield et al., 2016; Li et al., 2018; Kumar et al., 2020; Huang et al., 2022), have investigated the collision of two spherical drops.

When impact droplets collide with sessile droplets on the substrate, phenomena such as coalescence, expansion, and recoil occur depending on the relevant physical parameters (e.g., impact velocity and droplet size) and the fluid properties of the liquid (Wakefield et al., 2016).

With a substantial collision velocity of the droplet, the impact force is enhanced, which leads to a significant enhancement of the impact effect. This situation may lead to the breakup of droplets or the scattering of more tiny droplets. In addition, the droplet size significantly affects droplet impact behavior. When the droplet size is large, the droplet will appear more obvious deformation and deformation during the impact process, which has an impact on the impact dynamic characteristics. In contrast, smaller droplets are more prone to adhesion or

Nomenclature

We	Weber number	$\triangle t_2$	time intervals (0.2 ms) between the corresponding two frames
V_p	sessile droplet volume	τ	dimensionless time
V_i	impact droplet volume		downward compression displacement
Oh	Ohnesorge number	H_{max}	maximum height of the partial rebound of the liquid sheet
ρ	Density	D_f	maximum liquid crown diameter
σ	surface tension	H_f	corresponding liquid crown height
μ	viscosity coefficient	D_e	spreading diameter
d_h	horizontal diameter of droplets	H_e	liquid sheet height
d_v	vertical diameter of droplets	χ	dimensionless compression displacement
d_0	diameter of the spherical droplet	δ_{max}	maximum height of the partial rebound of the liquid sheet
v_0	impact velocity of the droplet	β_f	maximum liquid crown diameter
v_1	velocity of the first two frames of the droplet impacting the substrate	δ_f	liquid crown height
v_2	velocity of the last two frames of the droplet impacting the substrate	β_e	spreading diameter
$\triangle t_1$	time intervals (0.2 ms) between the corresponding two frames	δ_e	liquid sheet height

coalescence. In addition, the fluid's viscosity and surface tension play a substantial role in shaping the droplet impact dynamics. High viscosity fluid will reduce the fluidity of droplets, thus affecting the behavior after impact, while surface tension will affect the deformation and impact behavior of droplets. During the collision in the interaction of the droplet in motion and the stationary droplet, the interaction between droplets frequently occurs (Chen et al., 2022). Therefore, researchers consider the interaction between droplets by studying the collision of droplets with hemispherical droplets. Aiswal & Khanderkar (2021) conducted experimental investigations employing two distinct deposition methods to examine the impact performance of droplets on superhydrophobic surfaces. The study revealed that the deposition mode of sessile droplets on the substrate significantly influences the post-impact dynamics of droplets. Furthermore, the wetting behavior of droplets on the substrate also exerts a crucial influence on governing the processes of droplet rebound and coalescence during impact. Fujimoto et al. (2008) performed research investigations involving both experimental and numerical analyses of droplet collisions with hemispherical droplets on a horizontally smooth solid surface. A circular coronal thin liquid sheet formed around the base of the colliding droplets. The size of the circular film grew larger as the impact velocity increased. In addition, they investigated the deformation behavior of two droplets hitting a solid in succession. They took pictures with a CCD camera to understand the physics of the interaction between the two droplets. Raman et al. (2016) uses numerical simulations to model the collision behavior and interaction dynamics of droplets with initial gaps. The effects of droplet drag velocity, surface wettability, droplet viscosity, and surface tension on the time-varying dynamics during impact were investigated. Chen and Yang (2020) conducted a comprehensive direct numerical simulation of binary droplet collisions in dense spray dynamics. They developed and implemented an integrated numerical approach that merges the Adaptive Mesh Refinement (AMR) algorithm with the Volume of Fluid (VOF) interface tracking technique to deal with multi-scale flow physics of droplet collisions. Through a comprehensive parameter study of Weber number and collision parameter, they determined the bounce, merge, reflection separation and stretch separation states of droplet collisions. In addition, they developed a visualized method utilizing the ray tracing to obtain detailed insight into the physical process of droplet collisions. Chen et al. (2020) explored the dynamics of droplet interactions on a surface coated with a horizontal liquid sheet. The experimental study encompassed observations of droplet spreading, ejection, partial rebound, and full rebound in the aftermath of the impact event. Hamdan et al. (2015) Utilizing a high-speed camera, the spreading and fragmentation of impacting droplets were observed. When the Weber number of the droplets exceeded a certain threshold, evident from the observations with an escalation in the Weber number, a reduction in the dimensions of secondary droplets was noted.

Chen et al. (2017) examined the impact of droplet-wall film miscibility in the context of extremely thin films (0.02 times the droplet diameter). Their investigation revealed alterations in the formation of crowns and the threshold for splashing. For simulating the collision dynamics of droplets, an integrated approach is employed that combines the use of an innovative polynomial equation of state with the application of the Entropic Lattice Boltzmann Method (ELBM). This hybrid methodology is specifically designed to accurately simulate the complex interactions between two droplets under conditions characterized by high Weber and Reynolds numbers. (Moqaddam et al., 2016). Nikolopoulos et al. (2012) numerically investigated the nuclear binary impact of two droplets of unequal scale using the volume of fluid (V.O.F.) method. Quantitative analysis was performed to evaluate the impacts of Weber number (*We*), Ohnesorge number (*Oh*), droplet diameter ratios (*D*) on the generation of ligaments, maximum

deformation of both droplets, intrusion of one droplet into the other, and the formation of satellite droplets. They also presented a conducted empirical investigation aiming to explore the influence of a single water droplet on a stationary liquid block constructed from the previous impact of one or two droplets (Nikolopoulos et al., 2010). The corresponding qualitative and quantitative features regarding the evolution of this phenomenon over time were obtained through image analysis. Ma et al. (2019) investigated an empirical examination of the impacts of water droplets possessing varying Weber numbers (*We*) onto a water surface through experimental and numerical methods. Linear regression was utilized to assess the associations between *We* and the geometrical features of the central jet, secondary droplets, and secondary central jet.

Much of the research on a droplet colliding with another droplet on a substrate has focused on various phenomena arising from the interaction between two droplets. To comprehensively examine this phenomenon, some researchers have quantified its key characteristics for a more intuitive understanding. Kumar et al. (2020) investigated the merging kinetics of the partial coalescence phenomenon caused by a droplet colliding with a stationary droplet. They discussed the sessile and the relationship between the scale of the droplet that is impinging and the impact height or velocity (indicated by the Weber number) on the kinetics of partial coalescence. Using a high-speed camera, they experimentally investigated the kinetics of free-falling ethanol droplets onto sessile ethanol droplets under the influence of gravity, taking into account low impact heights (Weber numbers). He focused on the fusion of droplets and the generation of sub-droplets, and did not analyze the relevant characteristic parameters of droplet compression and liquid crown. In a study by Bernard et al. (2020), a comprehensive experimental analysis was conducted to understand the dynamics of crown-edge expansion in a system involving two droplets colliding with a wall membrane. The investigation focused on key metrics such as characteristic lengths, time scales, velocities, and accelerations. The researchers explored how these metrics were influenced by factors such as the thickness of the wall film, the initial impact velocity of the droplets, and the intrinsic properties of both the droplets and the wall film, including viscosity. They found that the maximum displacement of the crown is proportional relative to the velocity at which the droplets impacted. They analyzed the liquid crown, but did not consider the impact between the liquid drop and the liquid drop. Nikolopoulos et al. (2010) conducted experiments using two different film thicknesses, three different *We*, and two surface contact angles. Corresponding qualitative and quantitative features regarding the evolution of the phenomenon over time were obtained by image analysis. Analysis of the experimental data showed that the phenomenon has a strong similarity to the effect of a single droplet on shallow thin films.

As indicated by findings in the literature, the dynamics of droplet impact on sessile droplets leading to a non-splashing liquid crown and the phenomenon of non-coalescing downward compression deformation at the initial stage of droplet collision have not been studied. This lack of study serves as the motivation for the current work. We use high-speed photography to study the collision of deionized water droplets against stationary droplets of different volumes under different Weber numbers. Unlike Nikolopoulos et al. (2010), we consider the phenomenon of non-splattering liquid crowns. These are different from droplets hitting a horizontal liquid sheet, due to the effect of surface tension under high Weber number (*We*) conditions. Furthermore, we validate that in situations of low Weber number (*We*), the phenomenon of downward compression deformation is not merged in the initial stage of droplet collision. In addition, we also quantify the primary attributes of the aforementioned phenomena and study the influence stemming from the magnitude in relation to variations in the Weber number (*We*) and volume ratio (V_p/V_i).

2. EXPERIMENTAL SETUP

Figure 1 shows a schematic for the experimental setup. During the experiment, the whole impact process was recorded under the ambient conditions of 25°C temperature and 31% relative humidity. The main components comprising components such as a syringe pump, syringe barrel, pinhead, slide with adaptable pinhead positioning, and stainless steel substrate. In this experiment, the droplet generation device, lifting and sliding platform, supporting platform, and computer were positioned on an optical platform to minimize the influence of external vibrations. Before starting the experiment, several droplets were released consecutively to ensure stable droplet generation without air bubbles. Multiple droplets are generated by a 10-ml syringe driven by a syringe pump. The needle gauge is a standard 30 g flat needle, and the diameter of the generated droplets is 2.20 mm, and the corresponding error is ± 0.0152 mm. The lifting slide is employed to regulate the droplet's release height, generating moving droplets with distinct impact velocities. The lifting stage comprises both X and Y axes, with the X-axis aligned to the Z-axis of the vertical column. For precise adjustment of the droplet's lateral release position, a slider capable of lateral movement is incorporated into the X-axis. A needle holder is affixed to the slider to secure and maintain the needle in a vertical orientation. The sessile droplets are fixed on the stainless steel substrate. The substrate is mounted on a platform with an adjustable angle. The angle of the experimental platform is kept at 0 degrees. An electronic level is installed on the support platform to monitor the level of the wall. After the pendant droplet is generated by the pinhead tip, subject to gravitational influence, the droplet with a diameter of d_0 and a volume of V_i freely falls on a stationary droplet with a volume of V_p on a 110-mm × 90-mm × 6-mm stainless steel substrate. Each experiment was repeated more than five times to avoid randomness in the occurrence of correlated phenomena in the experiment. All data in the paper are the average of the measured data of each group of repeated experiments, and the error of the value of each group of repeated experiments and the average is 5% to 10%. We use the same needle to release sessile and impacting droplets (Kumar et al., 2020), ensuring the impacting droplet falls on the apex of the sessile droplet. The different heights of the needle are adjusted through the sliding table to control the different speeds of the impinging droplets. A high-speed video (Dimax HD, PCO, Germany, pixel size of 28μm) was employed to capture the complete collision sequence of numerous droplets at a speed of 5,000 frames per second (resolution

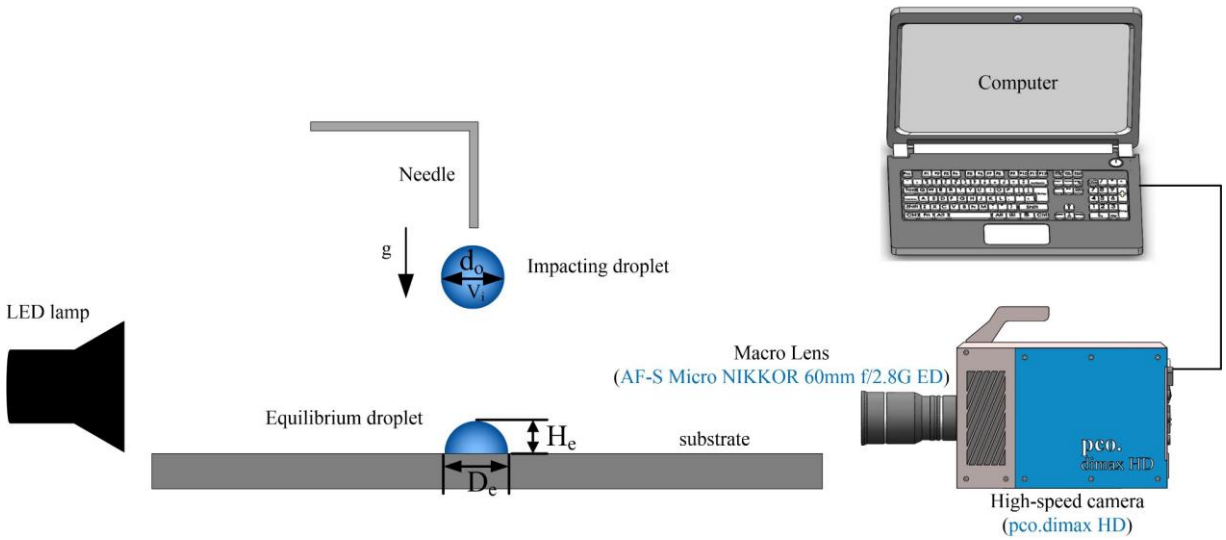

Fig. 1 Schematic diagram showing a freely falling droplet on a sessile droplet

960 × 424). A strong light was used to illuminate the background of the droplets.

The Weber number is commonly employed for characterize the rate of inertia force to capillary force during droplet impact, as follows:

$$We = \frac{\rho_l v_0^2 d_0}{\sigma} \tag{1}$$

In this experiment, deionized water was used as the experimental fluid. The dimensions and magnitudes of the colliding and stationary droplets are denoted by (d_0, V_i) and (D_e, V_p) correspondingly. The water has a density, ρ, of 997 kg/m^3, a surface tension, σ, equal to 0.073 N/m, and a viscosity coefficient, μ, measured at 1.005 mPa·s. MATLAB software and Python programming were used for pixel analysis to measure parameters such as droplet diameter, spread diameter, droplet height, liquid crown diameter, and liquid crown height. Calibration of measured images used 2 mm particles as a reference. Since the boundary of the figure is manually found to measure the relevant parameters through image recognition in this experiment, the operator's manual error is also taken into account. By comparing the results of the two users, it was found that the error in the obtained measurement results was less than 7%. Droplet diameter depends on inner diameter of the characteristics of the nozzle and the fluid's specific properties. Many studies on droplet oscillation pointed out that since the droplet oscillates when it falls, the droplet cannot maintain symmetry, and the droplet assumes an ellipsoidal shape as it descends., so its diameter is measured in the horizontal and vertical directions (Yoon et al., 2007; Chan et al., 2011; Li et al., 2018). The recorded horizontal diameter is denoted as d_h, while the vertical diameter is labeled as d_v. The size of the spherical liquid particle is defined by equation (2) (Li et al., 2018):

$$d_0 = \left(d_h^2 d_v\right)^{1/3} \tag{2}$$

Here, d_h and d_v represent the width and height of droplets, separately (Fig. 2a). Equation (3) defines the speed at which the droplet collides. (Li et al., 2018; Yang & Lee 2022):

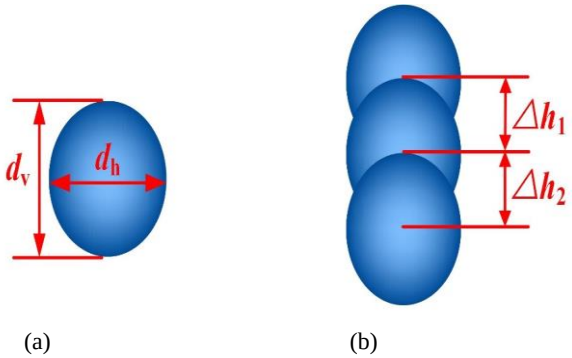

(a) (b)

Fig. 2 (a) Definition of horizontal diameter and vertical diameter of droplet (b) Displacement variation before droplet impact on substrate

$$v_0 = \frac{v_1 + v_2}{2} = \frac{1}{2}\left(\frac{\Delta h_1}{\Delta t_1} + \frac{\Delta h_2}{\Delta t_2}\right) \tag{3}$$

In equation (3), v_0 is the rate at which the droplet impacts, v_1 is the velocity of the first two frames of the droplet impacting the substrate, v_2 is the velocity of the last two frames of the droplet impacting the substrate, $\triangle t_1$ and $\triangle t_2$ are the time intervals (0.2 ms) between the corresponding two frames (Fig. 2b).

In addition, dimensionless time is defined by the relationship in equation (4) (Qin et al., 2019):

$$\tau = \frac{t v_0}{d_0} \tag{4}$$

Within this research, an array of tests were conducted to evaluate the performance of the droplet generator. The actual diameter of droplets produced under different Weber (*We*) conditions was measured and calculated using a 30-g flat needle. To ensure the accuracy of the experiments, each validation experiment was performed more than 30 times. The maximum measurement error is expressed by an error bar in Fig. 3. Figure 3 shows that droplet diameter remains nearly constant under different Weber (*We*) conditions.

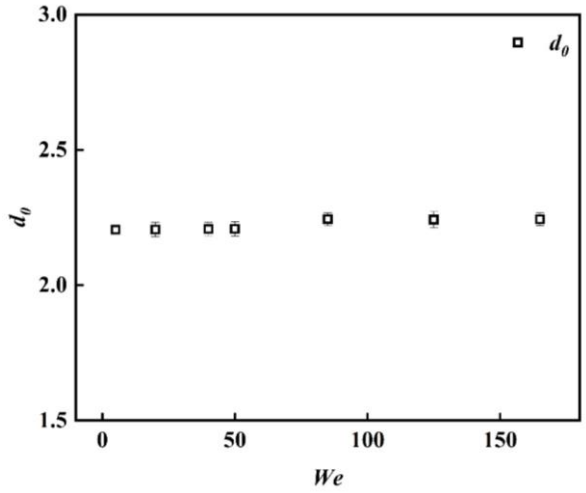

Fig. 3 The relationship between the actual diameter of impact droplet and drop *We*

For analyzing the deformation dynamics upon impact and providing a quantitative exploration of the factors that affect it, We define the downward compression displacement, Δh, and the maximum height of the partial rebound of the liquid sheet, H_{max}, in Fig. 4. In addition, the maximum liquid crown diameter, D_f, and the corresponding liquid crown height, H_f, spreading diameter, D_e, and liquid sheet height, H_e, at equilibrium after impacting the sessile droplet are also defined. The dimensionless compression displacement, $\chi=\Delta h / d_0$, maximum height of the partial rebound of the liquid sheet, $\delta_{max}=H_{max} / d_0$, maximum liquid crown diameter, $\beta_f=D_f / d_0$, liquid crown height, $\delta_f=H_f / d_0$, spreading diameter, $\beta_e=D_e / d_0$, and liquid sheet height, $\delta_e=H_e / d_0$, are obtained.

3. RESULTS AND DISCUSSION

The relevant physical properties considered in this investigation include droplet V_p/V_i (V_p is the sessile droplet volume, V_i is the impact droplet volume) and the impact droplet *We*. We systematically modify individual parameters while maintaining the other conditions constant to examine their influence on the non-splashing liquid crown and compression dynamics of the droplets. Over a large range of *We* variation, we investigate the phenomenon of a non-splashing liquid crown and the compression generated by a droplet's impact on a sessile droplet under high *We* conditions and different volume ratios (V_p/V_i). The relationships among the independent properties, V_p/V_i and *We,* and the dependent parameters, non-splashing liquid crown and compression generated by droplet collision, was studied. The maximum diameter, corresponding height, and compression displacement at the top of the liquid crown vary with *We* and V_p/V_i in the case of non-splashing and compression.

3.1 Evolution of Droplet Impact Process with Different Weber Numbers When $V_p/V_i = 1$

The first relationship involves studying the influence of *We* on the generation of a non-splashing liquid crown and compression. This is done through the utilization of a high-speed imaging device to record the process of the impacting droplet impacting the stationary droplet at six Weber numbers ranging from 1.5 to 165 when V_p/V_i =1. The Weber number is set to 1.5, 40, 50, 85, 125, and 165 by controlling the falling height of the collision droplet. Figure 5 shows the variation of the collision droplet generation a non-splashing liquid crown and the compression dynamics over time at different Weber numbers. The purpose of the diagram is to show the non-splashing liquid crown and compression behavior of the

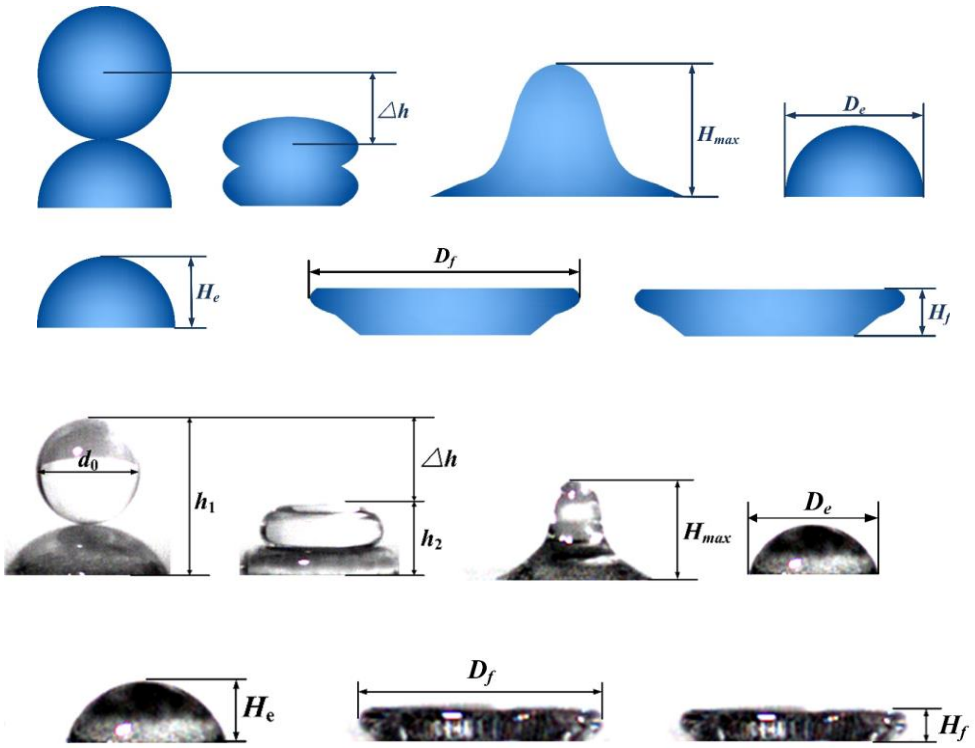

Fig. 4 Definition of the compression displacement

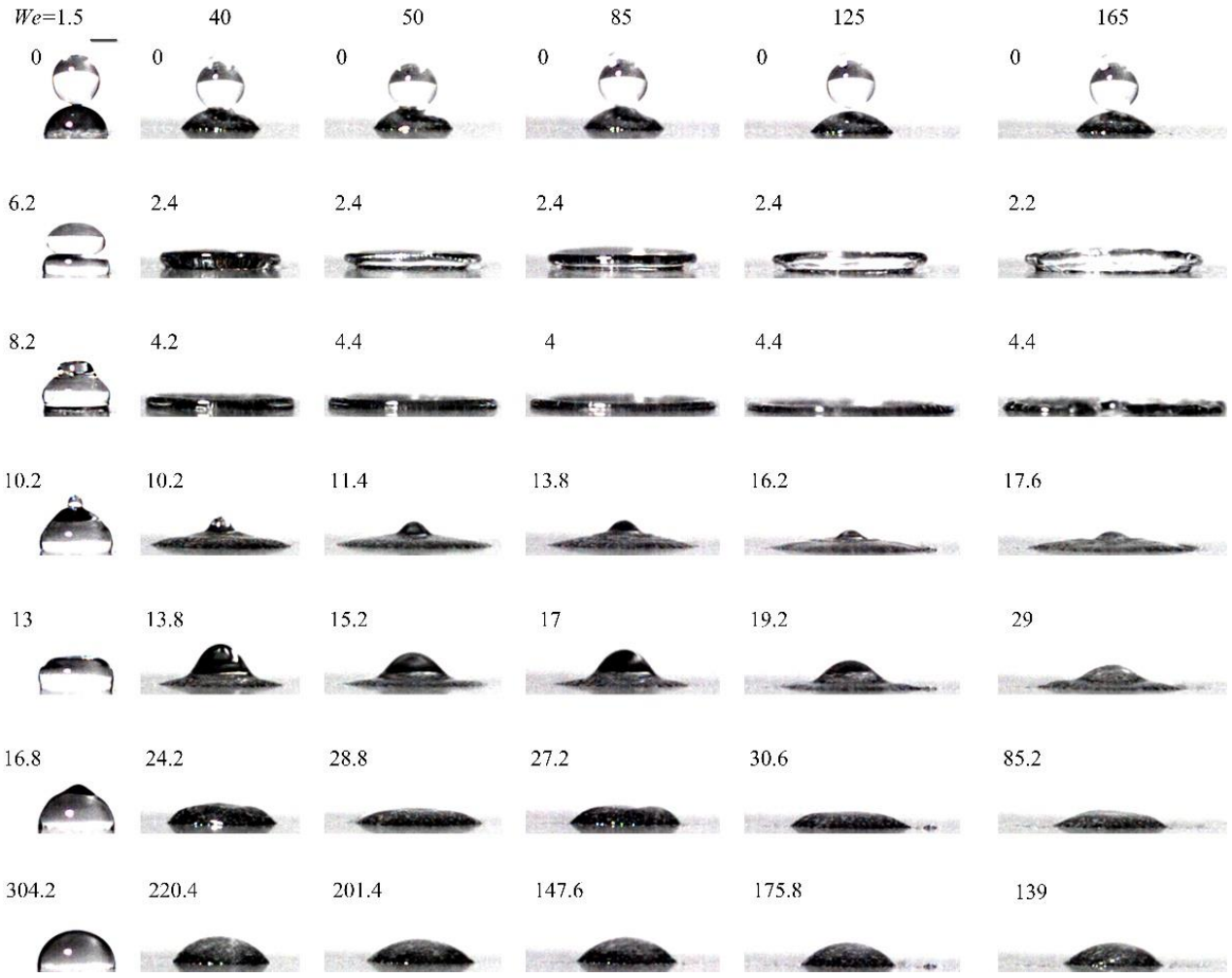

Fig. 5 The time evolution of impact droplets on sessile droplets for different We values at V_p/V_i =1

collision between a droplet in motion and a stationary droplet at various Weber numbers. For the results presented in this study, the moment of initial touch between the impacting droplet and the stationary droplet is defined as the starting time, labeled as t = 0 ms. The time (ms) is marked in the upper left corner of each frame in Fig. 5. The first row in Fig. 5 represents the case where the impact droplet contacts the sessile droplet (t = 0 ms). The following data displays the evolving coalescence and spreading behaviors of the droplets under various We values at different time intervals.

When *We* is set to 1.5 (the first column), the volume ratio of stationary droplets to impact droplets is 1. The droplets were compressed at the initial stage. Due to the existence of air between the two droplets, the impacting droplet did not coalescence with droplet at the initial stage of falling after contacting the sessile droplet. Instead, the mutual extrusion deformation occurred, and the two droplets form the shape of a round cake. Under these circumstances, the viscous force exerts greater influence than the capillary force, resulting in the damping of the capillary wave and the suppression of the coalescence after the collision of two droplets (Kumar et al., 2020). As the air discharged, the impacting droplet completely coalesces with the sessile droplet. As time progresses, the two droplets completely coalesce, and the droplet spreading diameter and height began to oscillate until finally reaching an equilibrium.

Figure 5 Columns 2 to 6 show the specific situation in which a droplet collides with a stationary droplet resulting in the formation of a liquid coronal structure during the collision stage. The time indicated in each image is denoted as t in milliseconds (ms), commencing from the instant of initial interaction between the impacting droplet and the stationary droplet. The scale bar illustrated in the upper-left corner of the initial panel corresponds to a distance of 1 millimeter (mm). The Weber number (*We*) corresponding to each column of images is marked separately at the top of the figure. Take the second column as an example, the droplet generates a liquid crown at the initial stage of the collision and gradually expands until the liquid crown reaches a maximum value (see t = 2.4 ms for *We* = 40). Then the liquid crown began to fall slowly, gradually spread, liquid sheet spreading diameter reached the maximum (see t = 4.2 ms for *We*=40). The fluidic layer initiates a rebounding motion as a result of the interaction between the liquid sheet and the underlying surface. (Ukiwe et al., 2005) (see t = 10.2 ms for *We* = 40). After reaching the maximum rebound height (see t = 13.8 ms for *We* = 40), the liquid sheet began to extend due to the effect of gravity. During a period time, the rebound and extending stages of liquid

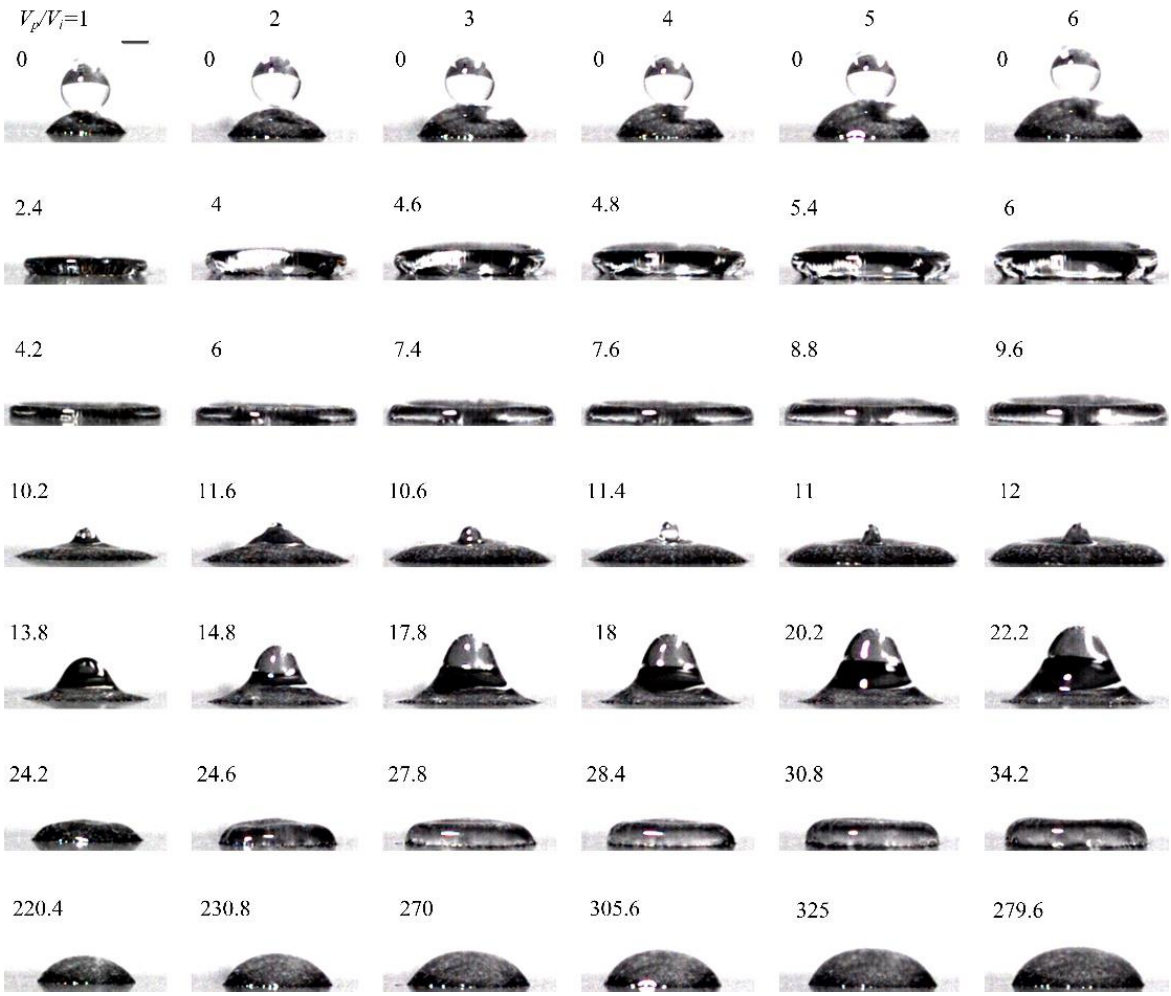

Fig. 6 The time evolution of impact droplets on sessile droplets for different volume ratios (V_p/V_i) values at *We* = 40

sheet alternated (see t = 24.2 ms for *We* = 40), until a spherical cap equilibrium state is reached on the substrate. It can also be seen from Fig.5 that when Weber number (*We*) reached a certain value, the edge of the liquid sheet formed a wavy shape (see t = 2.2 ms for *We* = 165), and the liquid sheet slowly backward began to spread, the spread of the liquid sheet edge also presents a wavy shape (see t = 4.4 ms for *We* = 165).

3.2 Evolution of droplet impact process with different volume ratio when *We* = 40

Over the range of *We*, we observed that, at *We* = 40, the droplet's impingement on the other droplet began to produce a non-splash liquid crown. Therefore, this behavior was tracked by changing the volume (V_p) of the stationary droplet to alter the volume ratios (i.e., V_p/V_i = 1, 2, 3, 4, 5, 6) at *We* = 40. The purpose is to study the effect of different volume ratios on the non-splashing liquid crown. The temporal evolutions of the impact droplets on stationary droplets for varying volume proportions (V_p/V_i) at *We* = 40 are presented in Fig. 6. The numerical value shown in each image corresponds to the time, denoted as t (ms), starting from the moment when the impacting droplet encounter the stationary droplet. The reference scale displayed in the upper left section of the illustration corresponds to a length of 1 mm. The volume ratio (V_p/V_i) corresponding to each column of images is marked separately at the top of the figure.

The process of how the droplet changes during collision with different volume ratios and a Weber number of 40 is similar. The droplet generates a liquid crown at the initial stage of the collision and gradually expands until the liquid crown reaches a maximum value. Owing to the interplay between surface tension and gravitational forces, the liquid crown began to fall slowly, gradually spread, and the liquid sheet spread diameter reached a maximum. Due to the role of repulsion between the liquid sheet and the substrate (Ukiwe et al., 2005), the liquid sheet began to bounce. Upon attaining the peak rebound altitude, the liquid sheet began to spread due to gravity. Throughout this time interval, the rebound and spreading stages of liquid sheet alternated until a spherical cap equilibrium state was reached on the substrate.

Figure 6 also demonstrates how, with the same *We*, an increase in volume ratio causes the highest recorded diameter of the non-splashing liquid crown generated by droplet impact to gradually increase. In addition, both the peak width of the liquid sheet spreading backward and the liquid sheet rebound height also increases. At the highest volume ratio of V_p/V_i = 6, the largest width of the liquid crown, the peak size of the spreading liquid sheet, and the maximum elevation of the liquid sheet rebound are the largest. This correlation arises due to the heightened influence of the interaction between the colliding droplet and the stationary droplet as the volume ratio of the droplets (V_p/V_i) increases.

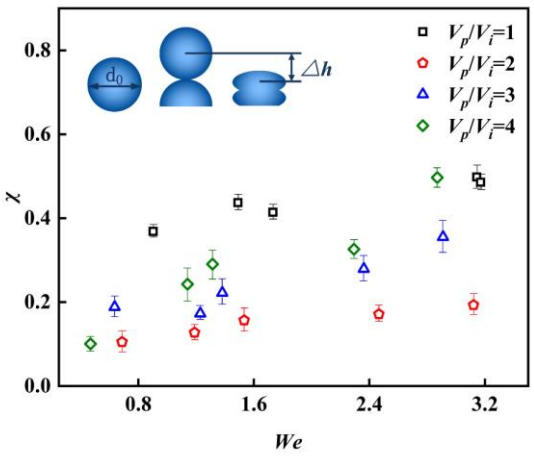

Fig. 7 Variations of the compression displacement (χ) with the We of the impacting droplet

3.3 Effect of Weber Number

Figure 7 shows the connection among the impact droplet displacement, χ, and the impact droplet *We* under different V_p/V_i. The displacement, χ, increases as the *We* increases. The maximum displacement is 0.5 at V_p/V_i = 1 for *We* = 3.14. The minimum displacement is 0.1 at V_p/V_i = 2 for *We* = 0.69. In addition, as the droplet V_p/V_i increases at a set *We*, the impact droplet displacement, χ, first decreases and then increases. During the process of impact droplet movement, an increase in the droplet volume resting on the substrate causes an increase in the surface tension of liquid sheet. In addition, the liquid sheet becomes increasingly difficult to compress, resulting in a decrease in impact droplet displacement, χ. According to previous research, when the displacement, χ, decreases to a certain extent, the volume of the droplet on the substrate continues to increase, and the area of the thin air layer involving the collision droplet and the stationary droplet also increases. With the same volume of impact droplets, it is more difficult for air to escape, so the displacement of the impact droplets increases (Chubynsky et al., 2020).

Figure 8(a) and (b) show the relationship between *We* and both the maximum liquid crown diameter (β_f) and the height (δ_f) of the liquid crown at different volume ratios (V_p/V_i = 1-6), respectively. With any V_p/V_i, a greater Weber number results in a greater liquid crown height (δ_f) and maximum diameter (β_f). In Fig. 8(a), When the values of V_p/V_i and *We* are lower, the liquid crown's maximum diameter, β_f, exhibits its minimum extent. That is, when V_p/V_i = 1 and *We* = 40, The smallest measurement for the liquid crown's maximum width (β_f) is noted at 2.23. The maximum width (β_f) of the predominant liquid crest dimension occurs when both the droplet's *Vp*/*Vi* ratio and the Weber number (*We*) are higher. That is, when V_p/V_i = 6 and *We* = 165, the maximum width (β_f) of the liquid crown is the largest at a value of 4.38. In Fig. 8(b), the minimum liquid crown height (δ_f) is 0.44 at V_p/V_i = 1 for We = 40, and the maximum liquid crown height (δ_f) is 1.19 at V_p/V_i = 6 for *We* = 165.

Furthermore, as depicted in Fig. 8(a), it is evident that the liquid crown diameter (β_f) increases with an increase in the V_p/V_i under the same *We* conditions. This phenomenon can be attributed to the fact that larger the capacity of the stationary droplet, the larger the total surface energy of the droplet system. In other words, the larger the total energy, the larger the maximum diameter (β_f) of the liquid crown during the spread process. After the maximum liquid crown is generated, the droplets began to fall back towards the substrate, and then spread until the maximum spreading diameter is reached. Most of the kinetic energy is converted into surface energy in this process, but it is reduced due to the loss of viscous force dissipation. This excess surface energy will eventually force the droplet to restore its equilibrium shape to a minimum energy configuration (Pittoni et al., 2014).

3.4 Effect of Volume Ratio

Figure 9(a) illustrates the relationship between the maximum droplet height (δ_{max}) and the ratio of droplet volumes (V_p/V_i = 1-6) with different Weber numbers. The maximum droplet height (δmax) correspondingly expands as droplet volume proportion (V_p/V_i) rises. When *We* = 165 and V_p/V_i = 1, the maximum height, δ_{max}, of the droplet is the smallest (0.5). When *We* = 40 and V_p/V_i = 5, the maximum height (δ_{max}) of the droplet is the largest at

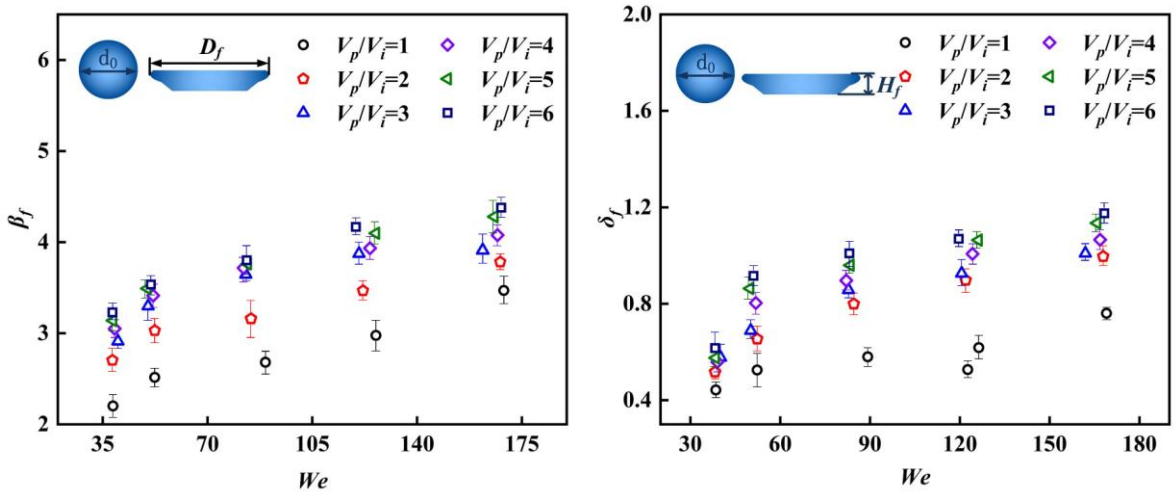

(a) (b)

Fig. 8 Effect of *We* on droplet characteristic parameters under certain volume ratio (V_p/V_i)

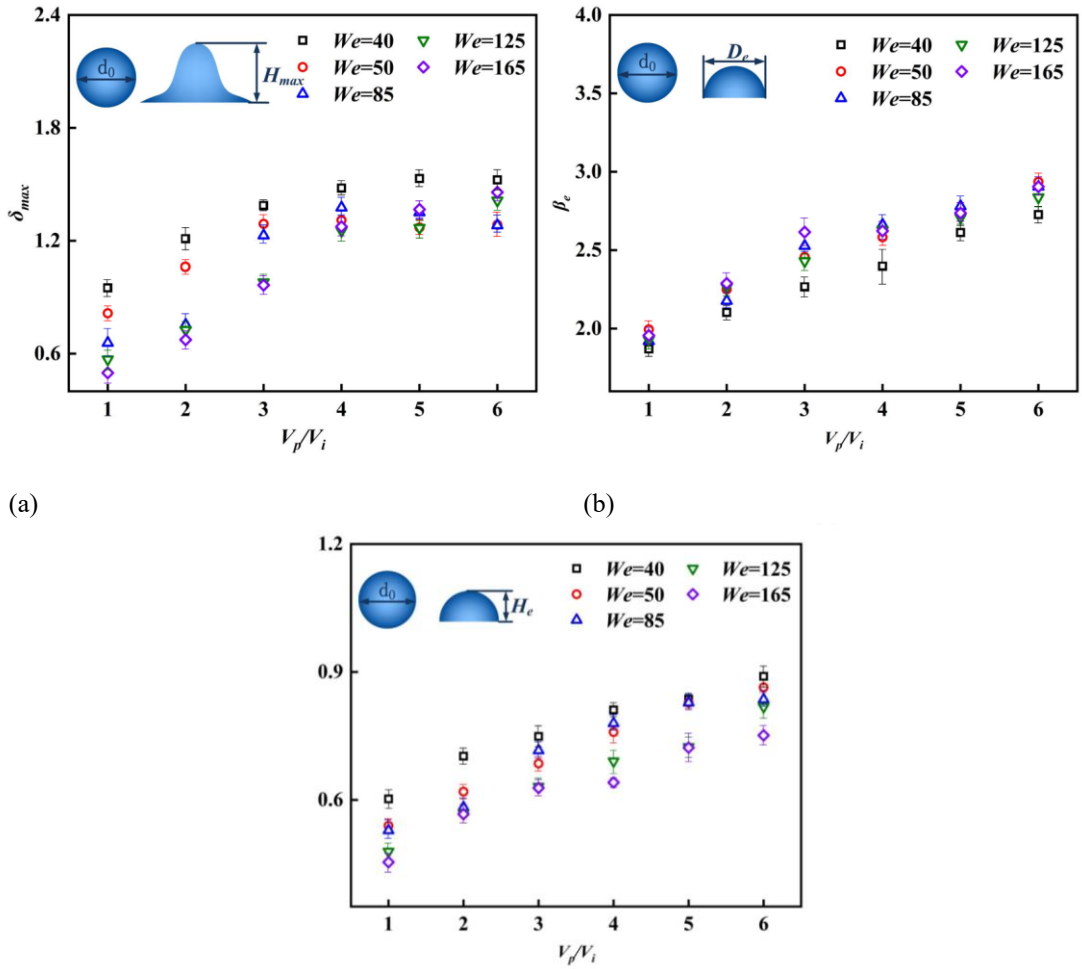

Fig. 9 Effect of volume ratio (V_p/V_i) on droplet characteristic parameters under different Weber numbers (*We*)

a value of 1.77. The vertical axis of the image illustrates how an elevation in the Weber number results in the maximum height (δ_{max}) of the droplet to first increase and then decrease. In addition, an increase in the droplet V_p/V_i leads to the gap between the maximum height (δ_{max}) of the droplet under different *We* becoming smaller. The larger the droplet V_p/V_i, the closer the maximum height (δ_{max}) of the droplet under varied Weber number conditions.

Figures 9(b) and (c) denote the relationship between the balanced diameter (β_e) and the balanced height (δ_e) of the droplet and the volume ratio (V_p/V_i = 1-6) under different *We*, respectively. With an increase in the V_p/V_i of the droplet, the balanced diameter (β_e) and balanced height (δ_e) of the droplet both increase. In Fig. 9(b), the equilibrium diameter (β_e) of the droplet increases with increasing *We* at the same V_p/V_i. When *We* = 50 and V_p/V_i = 1, the droplet equilibrium diameter is the smallest at 1.7 mm, and it reaches a maximum of 2.91 when *We* = 165 and V_p/V_i = 6. In Fig. 9(c), the equilibrium height of the droplet decreases with increasing Weber number at the same volume ratio. At V_p/V_i = 1 and *We* = 165, the minimum equilibrium height of the droplet becomes 0.49. At V_p/V_i = 6 and *We* = 40, the maximum equilibrium the droplet's vertical position alters 0.95.

Figure 10 shows the relationship between the utmost width (β_f) of the liquid crown as well as the corresponding height (δ_f) of the utmost width of the liquid crown and the volume ratio of the droplet (V_p/V_i = 1-6) under different Weber numbers. At different Weber numbers, a large V_p/V_i of the droplet results in a large largest dimension (β_f) and vertical extent (δ_f) of the liquid crown. A nonlinear relationship exists between the largest dimension of the liquid crown and the volume ratio, but the height of the largest dimension of the liquid crest and the volume ratio share a linear relationship.

In Fig. 10(a), when *We* = 40 and V_p/V_i = 1, the utmost width (β_f) of the liquid crown reaches a minimum of 2.25 but it reaches a maximum of 4.38 when *We* = 165 and V_p/V_i = 6. As the volume ratio increases, the highest diameter of the liquid crest first experiences a gradual increase. The rate of increase for the highest diameter of the liquid crest gradually decreases to form a plateau.

Figure 10(b) also shows how an increase in volume ratio leads to a larger gap between the highest point associated with the liquid crest to different Weber numbers at similar volume ratios. When the Weber number is large, the growth rate of the vertical extent of the liquid crest at its maximum point liquid crown decreases with the volume ratio (e.g., *We* = 165). However, when the impact droplet with a small Weber number collides with a sessile droplet, the vertical extent of the liquid crown at its maximum point liquid crown increases

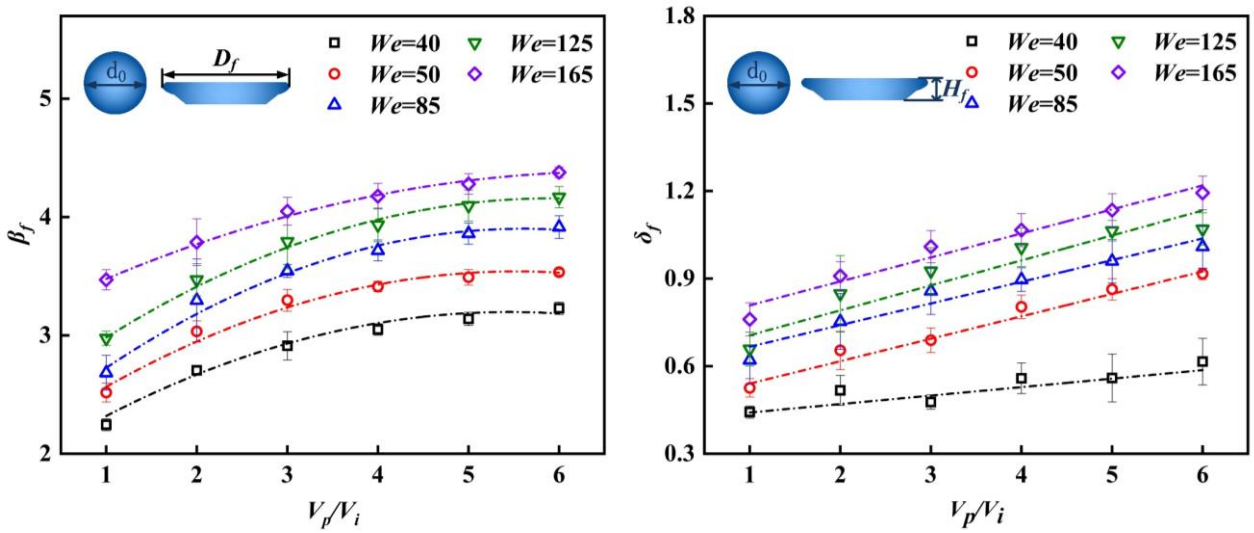

(a) (b)

Fig. 10 Effect of volume ratio (V_p/V_i) on droplet characteristic parameters during droplet spreading with different Weber numbers

slowly with an increase in the volume ratio. The main reason for these differences stems from how, with an increasing droplet volume ratio, the mass and inertia of the liquid escalates when the impact droplet interacts with the stationary droplet. Subjected to inertial force and capillary force, the peak diameter and the corresponding height of the liquid crown increase with increasing volume ratio.

4. CONCLUSIONS

In this experimental study, the phenomenon of impacting droplets colliding with sessile droplets of different volumes is studied by means of high-speed video. Based on the characteristics of droplet spreading, compression and non-splashing liquid crown, the observed phenomena and established principles in this study can be extended to $1 \leq We \leq 165$ and droplet volume ratios of $1 \leq V_p/V_i \leq 6$. The impacts of *We* on the droplet undergoing interaction and the V_p/V_i between the sessile droplet and the impact droplets regarding the dynamic behaviors exhibited by the droplets were studied. The dynamic behaviors of a droplet under different *We* and volume ratio were also studied. When $We < 4$, the droplet is compressed at the initial stage of collision. The droplet generated a non-splashing liquid crown during the collision when $We \geq 40$. Furthermore, this paper, focusing on the influence of the *We* and V_p/V_i on the typical characteristic parameters of droplets, explains the variation law of relevant characteristic parameters.

ACKNOWLEDGMENTS

This work is supported by the National Natural Science Foundation of China (Grant No. 52006198), the Key Research and Development Program of Zhejiang Province (Grant No. 2023C01171).

CONFLICT OF INTEREST

The authors have no conflicts to disclose.

AUTHOR CONTRIBUTIONS

Z. Lin and **D. Chen** conceived and designed the study. **D. Chen**, **L. Ming**, **TC**, and **M. Qiu** performed the experiments. **D. Chen** provided the mutants. **Z. Lin** and **D. Chen** wrote the paper. **Z. Lin**, **D. Chen**, **L. Ming**, **T. Wang** and **M. Qiu** reviewed and edited the manuscript. All authors read and approved the manuscript.

DATA AVAILABILITY

The data that support the findings of this study are available from the corresponding author upon reasonable request.

REFERENCES

Aiswal, A. K. J., & Khandekar, S. (2021). Dynamics of a droplet impacting a sessile droplet on a superhydrophobic surface :role of boundary conditions during droplet placement. *Journal of Flow Visualization and Image Processing, 28*(4), 69-89. https://doi.org/10.1615/JFlowVisImageProc.2021037109

Bai, C., & Gosman, A. D. (1995). Development of Methodology for Spray Impingement Simulation. *SAE Technical Papers*, 69-87. https://doi.org/10.4271/950283

Bernard, R., Vaikuntanathan, V., Weigand, B., & Lamanna, G. (2020). On the crown rim expansion kinematics during droplet impact on wall-films. *Experimental Thermal and Fluid Science*, *118*, 110168. https://doi.org/10.1016/j.expthermflusci.2020.110168

Chan, D. Y. C., Klaseboer, E., & Manica, R. (2011). Film drainage and coalescence between deformable drops and bubbles. *Soft Matter*, *7*(6), 2235-2264. https://doi.org/10.1039/C0SM00812E

Chen, B., Tian, R., & Mao, F. (2020). Analysis of special

phenomena of droplet impact on horizontal liquid film at low velocity. *Annals of Nuclear Energy*, *136,* 107038. https://doi.org/10.1016/j.anucene.2019.107038

Chen, D. S., Wang, T. T., Ming, L. N., Qiu, M., & Lin, Z. (2022) Dynamic characteristics of moving droplets impacting sessile droplets with different Reynolds numbers. *Physics of Fluids, 34* (11), 117120. https://doi.org/10.1063/5.0109293

Chen, N., Chen, H., & Amirfazli, A. (2017). Drop impact onto a thin film: Miscibility effect. *Physics of Fluids*, *29*(9), 1-7. https://doi.org/10.1063/1.5001743

Chen, X., & Yang, V. (2020). Direct numerical simulation of multiscale flow physics of binary droplet collision. *Physics of Fluids, 32*(6), 062103. https://doi.org/10.1063/5.0006695

Chubynsky, M. V., Belousov, K. I., Lockerby, D. A., & Sprittles, J. E. (2020). Bouncing off the walls: The influence of gas-kinetic and van der waals effects in drop impact. *Physical Review Letters*, *124*(8), 084501. https://doi.org/10.1103/PhysRevLett.124.084501

Dalili, A., Chandra, S., Mostaghimi, J., Fan, H., & Simmer, J. (2014). Formation of liquid sheets by deposition of droplets on a surface. *Journal of Colloid Interface Science, 418*, 292-299. https://doi.org/10.1016/j.jcis.2013.12.033

Deka, H., Biswas, G., Chakraborty, S., & Dalal, A. (2019). Coalescence dynamics of unequal sized drops. *Physics of Fluids, 31*, 012105. https://doi.org/10.1063/1.5064516

Emdadi, M., & Pournaderi, P. (2019). Study of droplet impact on a wall using a sharp interface method and different contact line models. *Journal of Applied Fluid Mechanics*, *12*(4), 1001-1012. https://doi.org/10.29252/jafm.12.04.29029

Farokhirad, S., Morris, J. F., & Lee, T. (2015). Coalescence-induced jumping of droplet: Inertia and viscosity effects. *Physics of Fluids, 27*(10), 1-15. https://doi.org/10.1063/1.4932085

Feng, J. Q. (2017). A computational study of high-speed microdroplet impact onto a smooth solid surface. *Journal of Applied Fluid Mechanics*, *10*(1), 243-256. https://doi.org/10.18869/acadpub.jafm.73.238.26440

Fujimoto, H., Tong, A. Y., & Takuda, H. (2008). Interaction phenomena of two water droplets successively impacting onto a solid surface. *International Journal of Thermal Sciences, 47*(3), 229-236. https://doi.org/10.1016/j.ijthermalsci.2007.02.006

Hamdan, K. S., Kim, D., & Moon, S. (2015). Droplets behavior impacting on a hot surface above the Leidenfrost temperature. *Annals of Nuclear Energy, 80*, 338-347. https://doi.org/10.1016/j.anucene.2015.02.021

Huang, Y. M., Sheng, Y. J., & Tsao, H. K. (2022). Peculiar encounter between self-propelled droplet and static droplet: swallow, rerouting, and recoil. *Journal of Molecular Liquids*, *347*, 118378. https://doi.org/10.1016/j.molliq.2021.118378

Karn, A., De, R., & Kumar, A. (2020). Some insights into drop impacts on a hydrophobic surface. *Journal of Applied Fluid Mechanics, 13*(2), 527-536. https://doi.org/10.2139/ssrn.3363043

Kumar, M., Bhardwaj, R., & Sahu, K. C. (2020). Coalescence dynamics of a droplet on a sessile droplet. *Physics of Fluids, 32*(1), 012104. https://doi.org/10.1063/1.5129901

Li, J., Huang, Z., & Liu, Q. (2018). Dynamics of a successive train of monodispersed millimetric-sized droplets impact on solid surfaces at low Weber number. *Experimental Thermal and Fluid Science*, *102*, 81-93. https://doi.org/10.1016/j.expthermflusci.2018.08.029

Li, P. F., Wang, S. F., & Dong, W. L. (2019). Capillary wave and initial spreading velocity at impact of drop onto a surface. *Journal of Applied Fluid Mechanics*, *12*(4), 1265-1272. https://doi.org/10.29252/JAFM.12.04.29614

Liang, G., Guo, Y., Shen, S., & Yu, H. (2014). A study of a single liquid drop impact on inclined wetted surfaces. *Acta Mechanica, 225*(12), 3353-3363. https://doi.org/10.1007/s00707-014-1110-8

Lim, T., Han, S., Chung, J., Chung, J. T., Ko, S., & Grigoropoulos, C. P. (2009). Experimental study on spreading and evaporation of inkjet printed pico-liter droplet on a heated substrate. *International Journal of Heat Mass Transfer*, *52*, 431-441. https://doi.org/10.1016/j.ijheatmasstransfer.2008.05.028

Luo, J., Wu, S. Y., Xiao, L., & Chen, Z. L. (2021). Parametric influencing mechanism and control of contact time for droplets impacting on the solid surfaces. *International Journal of Mechanical Sciences, 197*, 106333. https://doi.org/10.1016/j.ijmecsci.2021.106333

Ma, H., Liu, C., Li, X., Huang, H., & Dong, J. (2019). Deformation characteristics and energy conversion during droplet impact on a water surface. *Physics of Fluids*, *31*(6), 062108. https://doi.org/10.1063/1.5099228

Moghtadernejad, S., Lee, C., & Jadidi, M. (2020). An introduction of droplet impact dynamics to engineering students. *Fluids, 5*(3), 107. https://doi.org/10.3390/fluids5030107

Moqaddam, A., Chikatamarla, S. S., & Karlin, I. V. (2016). Simulation of binary droplet collisions with the entropic lattice Boltzmann method. *Physics of Fluids*, *28*(2), 1-21. https://doi.org/10.1063/1.4942017

Nikolopoulos, N., Strotos, G., Nikas, K. S., & Bergeles, G. (2012). The effect of Weber number on the central binary collision outcome between unequal-sized droplets. *International Journal of Heat and Mass Transfer*, *55*(7-8), 2137-2150. https://doi.org/10.1016/j.ijheatmasstransfer.2011.12.017

Nikolopoulos, N., Strotos, G., Nikas, K. S., & Gavaises, M., et al. (2010). Experimental investigation of a single droplet impact onto a sessile drop. *Atomization and Sprays*, *20*(10), 909-922.

https://doi.org/10.1615/AtomizSpr.v20.i10.70

Pittoni, P. G., Tsao, H. K., & Lin, S. Y. (2014). Water drop impingement on graphite substrates with random dilute defects. *Experimental Thermal and Fluid Science*, *53*, 142-146. https://doi.org/10.1016/j.expthermflusci.2013.11.021

Qin, M., Tang, C., Tong, S., Zhang, P., & Huang, Z. (2019). On the role of liquid viscosity in affecting droplet spreading on a smooth solid surface. *International Journal of Multiphase Flow*, *117*, 53-63. https://doi.org/10.1016/j.ijmultiphaseflow.2019.05.002

Raman, K. A., Jaiman, R. K., Lee, T. S., & Low, H. T. (2016). Lattice boltzmann study on the dynamics of successive droplets impact on a solid surface. *Chemical Engineering Science*, *145*, 181-195. https://doi.org/10.1016/j.ces.2016.02.017

Stone, H. A., Stroock, A. D., & Ajdari, A. (2004). Engineering flows in small devices: microfluidics toward a lab-on-a-chip. *Annual Review of Fluid Mechanics*, *36*, 381-411. https://doi.org/10.1146/annurev.fluid.36.050802.122124

Ukiwe, C., Mansouri, A., & Kwok, D. Y. (2005). The dynamics of impacting water droplets on alkanethiol self-assembled monolayers with co-adsorbed CH3 and CO2H terminal groups. *Journal of Colloid and Interface Science*, *285*(2), 760-768. https://doi.org/10.1016/j.jcis.2004.12.027

Wakefield, J., Tilger, C. F., & Oehlschlaeger, M. A. (2016). The interaction of falling and sessile drops on a hydrophobic surface. *Experimental Thermal and Fluid Science*, *79*, 36-43. https://doi.org/10.1016/j.expthermflusci.2016.06.022

Wang, L., Feng, J., Dang, T., & Peng, X. (2021). Dynamics of oil droplet impacting and wetting on the inclined surfaces with different roughness. *International Journal of Multiphase Flow*, *135*, 103501. https://doi.org/10.1016/j.ijmultiphaseflow.2020.103501

Yang, J., & Lee, C. (2022). Experimental study on phenomena of single water droplet impacts on liquid surfaces: Pattern maps and correlations. *Experimental Thermal and Fluid Science*, *130*, 110480. https://doi.org/10.1016/j.expthermflusci.2021.110480

Yoon, Y., Baldessari, F., Ceniceros, H. D., & Leal, L. G. (2007). Coalescence of two equal-sized deformable drops in an axisymmetric flow. *Physics of Fluids*, *19*(10), 102102. https://doi.org/10.1063/1.2772900

Zhong, Y., Dong, X., Yin, Z., & Fang, H. (2020). Theoretical design of inkjet process to improve delivery efficiency. *Journal of Applied Fluid Mechanics*, *13*(1), 275-286. https://doi.org/10.29252/jafm.13.01.30395